JOURNAL OF APPLIED ELECTROCHEMISTRY 24 (1994) 619–625

# Experimental comparison of electrochemical and dot-paint methods for the study of decaying swirling flow

H. AOUABED, P. LEGENTILHOMME, C. NOUAR*, J. LEGRAND

*Laboratoire de Génie des Procédés-I.U.T., BP 420–44606 Saint-Nazaire Cedex, France*

Received 13 May 1993; revised 22 September 1993

Swirling decaying flow in an annular cell fitted with a tangential inlet equal in diameter to the gap width was experimentally investigated. The attention was focused on the local flow field on both cylinders, the structure of which was determined using two experimental techniques: wall shear stress measurements achieved by means of the limiting electrodiffusional current on microelectrodes and a wall visualization method, the so-called dot-paint method which was used in order to determine the flow direction. This study showed the complex structure of the flow field just downstream of the tangential inlet, where a recirculation zone is set up, the effects of which are more sensitive on the inner cylinder, and the flow structure can be considered as three-dimensional in the whole entrance section.

**List of symbols**

$A$ microcathode surface area ($m^2$)
$C$ potassium ferricyanide concentration ($mol\,m^{-3}$)
$d$ microelectrode diameter (m)
$D$ ferricyanide ion diffusion coefficient in the mixture ($m^2\,s^{-1}$)
$e$ thickness of the annular gap, $R_2 - R_1$ (m)
$F$ Faraday constant ($96\,487\,C\,mol^{-1}$)
$I_L$ limiting diffusional current (A)
$k$ local momentum transfer coefficient ($m\,s^{-1}$)
$l_{out}$ entrance length on the outer cylinder (m)
$R_1$ external radius of the inner cylinder (m)
$R_2$ internal radius of the outer cylinder (m)
$Re$ Reynolds number, $2eU_m/\nu$
$s$ velocity gradient ($s^{-1}$)
$S$ swirl number
$s_{ax}$ velocity gradient obtained in fully developed axial flow ($s^{-1}$)
$s_{df}$ velocity gradient measured in developing axial flow ($s^{-1}$)
$s_{in}$ velocity gradient on the inner cylinder ($s^{-1}$)
$s_{out}$ velocity gradient on the outer cylinder ($s^{-1}$)
$T$ time average resulting velocity ($m\,s^{-1}$)
$U$ time average axial velocity component ($m\,s^{-1}$)
$U_m$ mean axial velocity in the annular gap ($m\,s^{-1}$)
$W$ time average tangential velocity component ($m\,s^{-1}$)
$x$ axial distance from the tangential inlet (m)

*Greek letters*

$\phi_e$ diameter of the tangential inlet (m)
$\nu$ kinematic viscosity of the working solution ($m^2\,s^{-1}$)
$\rho$ density of the working solution ($kg\,m^{-3}$)
$\psi$ angle with respect to the tangential inlet axis (degree)
$\theta$ angle of the streamline with respect to the horizontal (degree)

## 1. Introduction

Swirling flows result from the application of a tangential velocity component to the main axial movement of a fluid. Such flows can be classified into two different types according to the technique employed to induce the rotation of the fluid [1]: (i) continuous swirl, which persists along the flow path, can be achieved by twisted tapes [2] or coiled wires [3]; (ii) swirling decaying flows, induced by tangential inlets, helical inserts, inclined vanes, etc. [1], for which the swirling effect is generated at the entrance section and thereafter decays freely along the flow path. This second kind of swirling motion, induced by tangential inlets, because of the beneficient effects of the circumferential velocity component, easy maintenance and simple design, is used in several engineering devices such as heat exchangers [4], providing economy in space and enhancement in heat transfer in comparison with that obtained in axial pipe flow. Another area of application deals with the improvement of electrochemical metal removal from dilute solutions [5].

In previous work [6, 7], we have measured the overall mass transfer on the inner core of an annulus fitted with a tangential inlet of various diameter, $\phi_e$, with respect to the annular gap thickness, $e$. According to the value of the ratio $\phi_e/e$, we distinguished three kinds of swirling motions which differ hydrodynamically: (i) so-called pure swirl flow, which has been extensively investigated by Legentilhomme and Legrand [6], when $\phi_e/e = 1$. Overall mass transfer

This paper was presented at the International Workshop on Electrodiffusion Diagnostics of Flows held in Dourdan, France, May 1993.

*Present address: LEMTA–CNRS–URA 875, 2 Avenue de la Forêt du Hay, 54504 Vandœuvre Cedex, France

0021-891X 

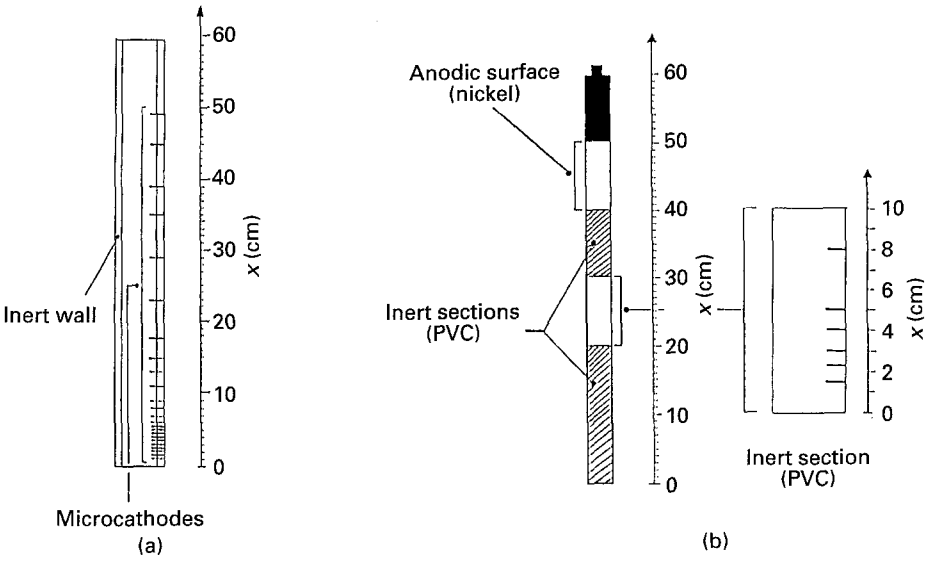


Fig. 1. Sketch of the electrochemical cell: (a) outer cylinder, (b) inner cylinder.

coefficients have been found to decrease along the flow path, because of the decay in swirl intensity, and to increase with both the axial Reynolds number, $Re$, and the initial swirl intensity. Enhancement in mass transfer up to 500%, in comparison with fully developed axial flow, can be achieved using such a swirling motion; (ii) when $\phi_e/e > 1$ (contraction swirl flow), overall mass transfer coefficients decrease with an increase in $\phi_e$, for identical axial location and Reynolds number, due to a decrease in initial swirl intensity [7]; (iii) in the expansion swirl flow, $\phi_e/e < 1$, a recirculation zone is set up just downstream of the tangential inlet [7].

Despite the fact that backflows cannot be detected in pure and contraction swirling motions, using our overall mass transfer measurements, we have predicted this flow pattern numerically employing an implicit finite difference algorithm in order to solve the Navier–Stokes and convection-diffusion equations previously reduced using boundary layer hypothesis [8]. In the range of geometric and hydrodynamic parameters of the experimental configurations [6, 7], the simulation showed negative axial velocity component near both cylinders just downstream of the tangential inlet. Local measurements of velocity gradients on the outer cylinder [10], achieved by means of the limiting electrodiffusional current on circular microelectrodes, do not support this hypothesis.

Because of this apparent contradiction, the present study is dedicated to a deeper investigation of the flow patterns on both cylinders of a cell fitted with a tangential inlet equal in diameter to the annular gap (pure swirl flow). Two experimental methods are employed: (i) the electrochemical method is used to measure wall shear stress on microelectrodes embedded axially along both cylinders; (ii) a visualization technique, the so-called dot-paint method, allowing a comparison with velocity gradient data.

## 2. Experimental details

### 2.1. *General setup*

A schematic flow diagram is shown in [7]. The annular test section was made from an Altuglas outer tube with 25 mm internal radius, $R_2$. The inner cylinder had an external radius, $R_1$, of 18 mm. The electrochemical cell used for wall shear stress measurements was 600 mm long. The inner cylinder was made of different parts, one of them supporting the microelectrodes (see Section 2.2 and Fig. 1(b)), another acting as anode. For the flow visualization experiments, the cell was 390 mm long, the inner cylinder consisting of a single PVC element. These two cells were fitted with a 7 mm tangential inlet in order to produce a pure swirling motion ($\phi_e = e$).

### 2.2. *Wall shear stress measurements*

To measure the velocity gradients, nickel microcathodes were placed on both cylinders of the annular cell. Embedded axially along the outer cylinder were 23 microelectrodes; six were placed on a 100 mm long PVC element which could be moved along the inner core of the annulus. The locations of the microcathodes on both cylinders are given in Fig. 1. Each microelectrode consisted of the cross-sectional area of a nickel wire 0.4 mm in diameter. The local electrochemical measurements were carried out using a polarographic method involving the reduction of ferricyanide ions at the nickel microcathodes. More details of this technique can be found in [7]. The working liquid was a mixture of 0.5 M sodium hydroxide, acting as supporting electrolyte, $2 \times 10^{-3}$ M potassium ferricyanide and $5 \times 10^{-2}$ M potassium ferrocyanide. The experiments were carried out at a constant temperature of 30 °C; the electrolyte density was $\rho = 1030\,\mathrm{kg\,m^{-3}}$, its kinematic viscosity $\nu = 8.73 \times 10^{-7}\,\mathrm{m^2\,s^{-1}}$ and the diffusion coefficient of the ferricyanide ions in the mixture $D = 6.95 \times 10^{-10}\,\mathrm{m^2\,s^{-1}}$. The experimental facility, including an electronic circuit with a multiplexer and a potentiostat, was the same as that used by Legrand *et al.* [9] to investigate wall shear stress on the outer cylinder. The mean limiting current, $I_L$, measured at each microcathode, working in inert

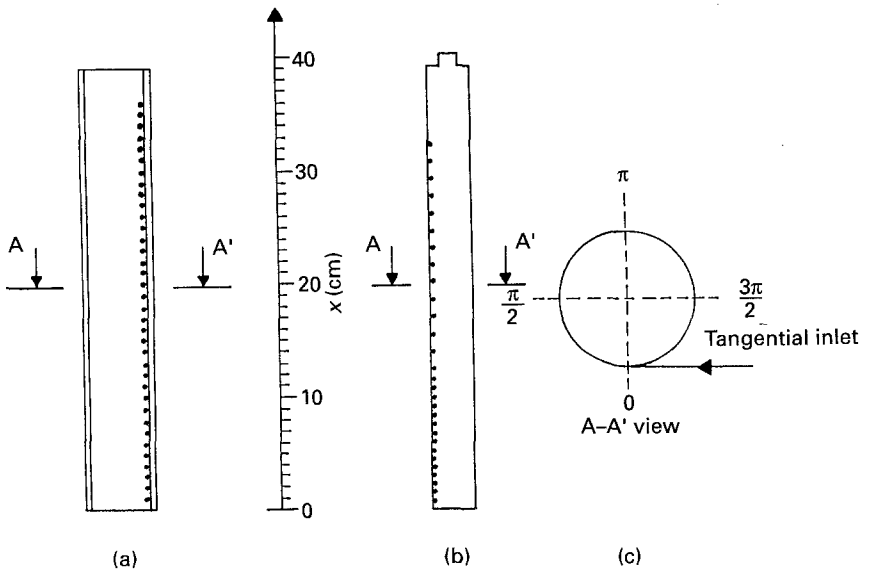


Fig. 2. Sketch of the visualization cell: (a) outer cylinder, (b) inner cylinder, (c) sectional view.

wall, led to a local momentum transfer coefficient, $k_F$. Reiss and Hanratty [10] have shown that $k_F$ and the velocity gradient, $s$, on a circular microelectrode of diameter $d$, are related by the following equation:

$$k_F = \frac{I_L}{FAC_s} = 0.862\left(\frac{D^2 s}{d}\right)^{1/3} \quad (1)$$

where $A$ is the microcathode surface area, $F$ is Faraday's constant and $C_s$ is the potassium ferricyanide concentration in the solution.

The microelectrodes were first calibrated under developed laminar axial flow conditions, for which s can be calculated from the Poiseuille velocity profile.

### 2.3. *Flow visualization experiments*

In order to test the flow patterns detected using wall shear stress measurements, a wall flow visualization technique was used, the so-called dot-paint method. This technique is intended to enable the nature of the flow over the surface of both cylinders of the annular cell to be investigated. The surface of both cylinders was coated with white paint (+ + +105 Titanium White PW6/PW4) at regularly spaced points (see Fig. 2). A suitable oil medium (Velocity 3 from Mobil Oil), mixed with a certain amount of dispersing agent (Rembrand Painting Medium 0.83), was used as working liquid. The fluid flowing over the surface carries the oil with it and a streaky deposit of paint remains to mark the direction of the flow. The patterns made by the streaks indicate the mean local directions of flow on both cylinders of the annular gap. The disposition of the paint spots are given in Fig. 2. In order to investigate the general flow structure in the three-dimensional field, paint spots were located axially at different angles, $\psi$, with respect to the axis of tangential inlet (see Fig. 2). $\psi$ was equal to 0, $\pi/2$ and $3\pi/2$ on the inner cylinder and 0, $\pi$ and $3\pi/2$ on the outer one. The flow patterns were photographed using an Olympus 101 camera allowing the measurement of the angle of the steamlines for different axial locations and Reynolds numbers.

## 3. Flow pattern on the outer cylinder

### 3.1. *Wall shear stress results*

The measurements of velocity gradients, $s_{out}$, on the outer cylinder have been extensively analysed in [9] for both laminar and turbulent swirling flow regimes. The experimental domain covered by Legrand *et al.* [9] was defined by: $90 \leqslant Re \leqslant 3\,780$ and $0.7 \leqslant x/2e \leqslant 35$, $x$ being the axial location of the microcathodes from the tangential inlet. In Fig. 3, the data are shown in terms of $s_{out}/s_{ax}$ as a function of $x/2e$. $s_{ax}$ is the developed axial velocity gradient calculated using the developed axial velocity profiles given by Ross and Wragg [11] in both laminar and turbulent flow regimes.

In Fig. 3, two kinds of wall shear stress development are seen according to the value of the dimensionless axial distance. For $x/2e \leqslant 13$, $s_{out}/s_{ax}$ decreases very sharply with $x/2e$, due to the combination of two phenomena: (i) the decay in swirl intensity; (ii) the entrance effects. For $x/2e \geqslant 13$, the velocity gradient decrease is weaker and can only be related to the final decay of the swirling motion. In [9], the experimental data have been correlated, in laminar swirling flow regime ($Re \leqslant 1000$), by the following relations:

For $x/2e \leqslant 13$:

$$\frac{s_{out}}{s_{ax}} = 6.30 Re^{0.54}\left(\frac{x}{2e}\right)^{-1.4} \quad (2)$$

For $x/2e > 13$:

$$\frac{s_{out}}{s_{ax}} = 98.7 Re^{0.05}\left(\frac{x}{2e}\right)^{-1.0} \quad (3)$$

For $x/2e \leqslant 13$, the values of the velocity gradients in swirling decaying flow are significantly higher than those obtained in developed axial flow (Fig. 3). The real increase in the momentum transfer due to the tangential velocity component has been evaluated in [9], calculating the ratio of the swirl and the developing axial, $s_{df}$, wall velocity gradients. The following

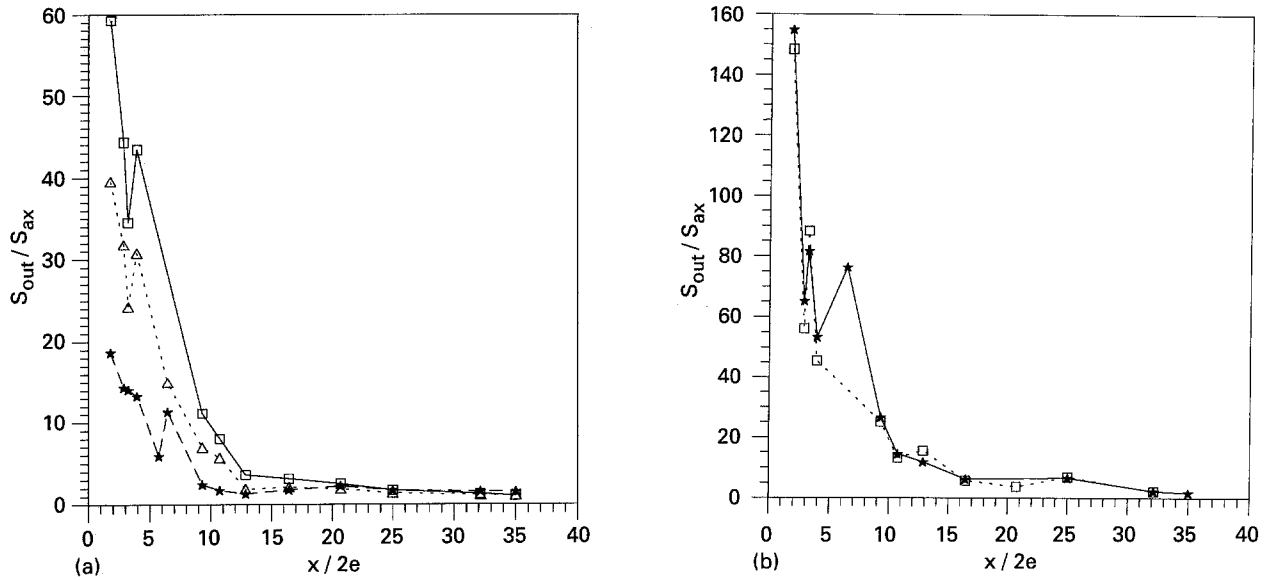


Fig. 3. Variation of velocity gradients on the outer cylinder in terms of $s_{out}/s_{ax}$ as a function of the dimensionless axial location, $x/2e$: (a) laminar flow regime, (b) turbulent flow regime (after [9]). Reynolds number, $Re$: (★) 92, (△) 311 and (□) 514 for (a); (★) 3060 and (□) 3775 for (b).

equation for $x/2e \leqslant 13$ was obtained:

$$\frac{s_{out}}{s_{df}} = 16.50 Re^{0.28} \left(\frac{x}{2e}\right)^{-1.1} \tag{4}$$

Using Equation 3, the entrance length, $l_{out}$, may be calculated in order to obtain a velocity gradient in swirling flow equal to 90% of the developed axial value ($s_{out}/s_{ax} = 0.9$). $l_{out}$ is given by

$$\frac{l_{out}}{2e} = 109.7 Re^{0.05} \tag{5}$$

### 3.2 *Flow visualization results*

To express the decrease in swirling intensity along the flow path, the angle, $\theta$, of the streamlines on the outer cylinder, with respect to the horizontal, was measured as a function of the reduced axial location, $x/2e$. The range covered by the experimental parameters was $1.1 \leqslant x/2e \leqslant 25.5$ and $100 \leqslant Re \leqslant 2000$. Figure 4 shows the variation of $\theta$ as a function of $x/2e$ for different values of the Reynolds number for $\psi = 0$. Two zones are apparent, according to the value of $x/2e$, for which the flow pattern appears very different: (i) near the tangential inlet (for $x/2e \leqslant 13$), the streamline angles do not increase monotically. A periodic behaviour occurs for which $\theta$ sharply increases and thereafter decreases; this reveals secondary vortices at the lower end of the cell. This region, where the swirl decay is not monotonic, was also observed during wall shear stress experiments (see Fig. 3(a) and (b)), for which the evolution of $s_{out}$ presents extrema during the decrease. The differences in the location of the extrema for angle and $s_{out}$ measurements can be attributed to non-coincidence of the measurement points circumferentially with the two experimental methods. (ii) for $x/2e > 13$, $\theta$ increases monotonically towards 90° when the flow becomes mainly axial at the end of the cell. On Fig. 4, for a given axial location, $\theta$ tends more rapidly towards 90° for smaller values of $Re$, due to the decrease in initial swirl intensity [7, 9]. This fact is in good agreement with velocity gradient data.

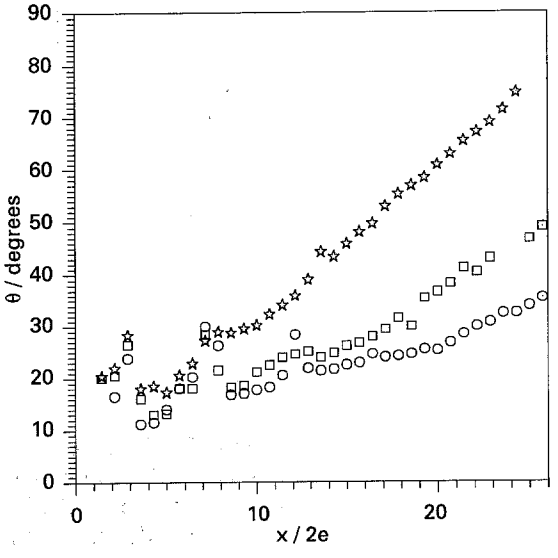


Fig. 4. Variation of the streamline angle, $\theta$, as a function of $x/2e$, for $\psi = 0$, on the outer cylinder. Reynolds number, $Re$: (★) 462, (□) 1194 and (○) 1994.

In Fig. 5, $\theta$ is plotted, as a function of $x/2e$, for $Re = 1990$, and the three values of the angle $\psi$ with respect to the tangential inlet axis. At the lower end of the annulus, $\theta$ strongly depends on the circumferential position, which reflects the three-dimensional flow field downstream of the tangential inlet. This flow pattern has previously been observed by Hay and West [12] for swirling decaying flow in a pipe induced by a tangential rectangular inlet and by Yukawa and Hashimoto [13] in an annular cell fitted with the same type of swirl generator. As the liquid reaches the top of the cell, the flow field becomes axisymmetric (for $x/2e \geqslant 17$ in Fig. 5). The axial position for which we can consider that the swirling motion

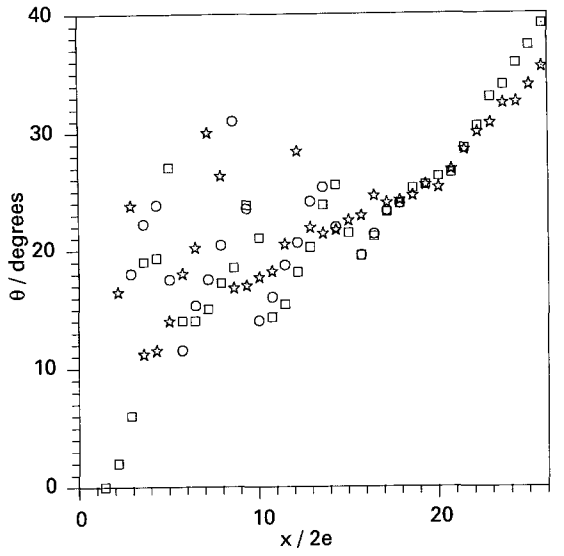


Fig. 5. Influence of the circumferential location, $\psi$, on the streamline angle, $\theta$, for $Re = 1990$ on the outer cylinder. $\psi$: (□) 0, (☆) $\pi$ and (○) $3\pi/2$.

has lost its three-dimensional character increases with an increase in Reynolds number, due to the larger initial swirl intensity. The angle $\theta$, measured on the outer cylinder, is always positive whatever $x/2e$, $Re$ and $\psi$. This fact is in apparent disagreement with our simulation of such a flow, for which a recirculation zone, characterized by negative axial velocities on both cylinders, just downstream of the tangential inlet was predicted [8]. It seems possible that these backflows only occur, on the outer cylinder, in the immediate vicinity of the swirl generator, where it is difficult to employ the dot-paint method successfully to investigate the flow field.

To determine the hydrodynamic entrance length, $l_{out}$, for which $\theta$ is equal to 90% of its value in axial flow ($\theta_0 = 90°$), experimental values of $\theta$ have been correlated as a function of $Re$ and $x/2e$, the latter parameter expressing the incidence of the decaying swirl intensity. To set up this correlation, only data points for which $\theta$ can be considered to increase monotonically and independent of the tangential position $\psi$ are included. For 420 experimental points, the following correlation was obtained using a multilinear regression algorithm:

$$\frac{\theta}{\theta_0} = 0.60 Re^{-0.42} \left(\frac{x}{2e}\right)^{0.87} \tag{6}$$

from which

$$\frac{l_{out}}{2e} = 1.60 Re^{0.48} \tag{7}$$

Equation 7 is very different from that giving $l_{out}$ in terms of wall velocity gradient (Equation 5). This fact points out the interest of using two different experimental methods to study the local flow field: the measured velocity gradient is characteristic of the resulting velocity gradient on the outer cylinder (a combination of the axial and tangential velocity components), whereas the dot-paint method allows the determination of the direction of the flow. Thus we can measure a velocity gradient very close to that obtained in developed axial flow whereas the flow field remains dominated by the tangential velocity component. This was previously shown in [8]; the axial wall velocity gradient in the monotonic swirling decaying flow may be smaller than that obtained in developed axial flow. But the resulting velocity gradient may be equal or greater due to the tangential velocity component.

In decaying swirl flow, the degree of swirl is often characterized by the swirl number, S, which is a dimensionless parameter defined by the ratio of the axial flux of swirl momentum, $G_\theta$, to the product of axial flux of axial momentum, $G_x$, by the equivalent tube radius, $R$ (Gupta *et al.* [1]). Taking $R_1$, the radius of the inner cylinder, as $R$, $S$ is given by

$$S = \int_{R_1}^{R_2} \frac{UWr^2 dr}{R_1 U^2 r dr} \tag{8}$$

$U$ and $W$ being the time average axial and tangential velocity components, respectively.

Edwards *et al.* [14] found that $U$ and $W$ can be written as a function of $\theta$ and of the resulting velocity, $T$, as follows:

$$U = T \sin\theta \tag{9}$$

$$W = T \cos\theta \tag{10}$$

Assuming that $T$ may be considered as independent of $r$ in the region where $\theta$ increases monotonically along the flow path, and taking into account that $\theta$, $U$ and $W$ are related by $U/W = \tan\theta$, Equation 8 can be integrated to give

$$S = \frac{\sin 2\theta (R_2^3 - R_1^3)}{3 \sin^2\theta (R_2^2 - R_1^2) R_1} \tag{11}$$

The hypothesis of the constancy of $T$ can only be used to first approximation, but it is supported by the fact that $s_{out}/s_{ax} \simeq 1$ when $\theta$ increases monotonically, which means that the resulting velocity, governing the wall gradient, is nearly constant. Using Equation 11, $S$ has been determined for the 420 experimental data used to set up Relation 6.

Hay and West [12] found that the decrease in $S$ with $x$ is predicted by the empirical relation $S = a \exp(-bx)$. This experimental result was confirmed by the theoretical work of Benisek *et al.* [15, 16] in the laminar flow regime and that of Kito and Kato [17] in turbulent swirling flow. Thus $S$ has been correlated by the following relation:

$$S = 0.13 Re^{0.56} \exp\left(-0.08 \frac{x}{2e}\right) \tag{12}$$

Equation 12 is given with a mean square error of 20% which is mainly due to the higher values of $Re$ ($Re \geqslant 1200$) for which $\theta$ only increases monotonically towards 90° for the last few axial locations.

## 4. Flow pattern on the inner cylinder

### 4.1. *Wall shear stress results*

In Fig. 6, the ratio of the velocity gradient measured in

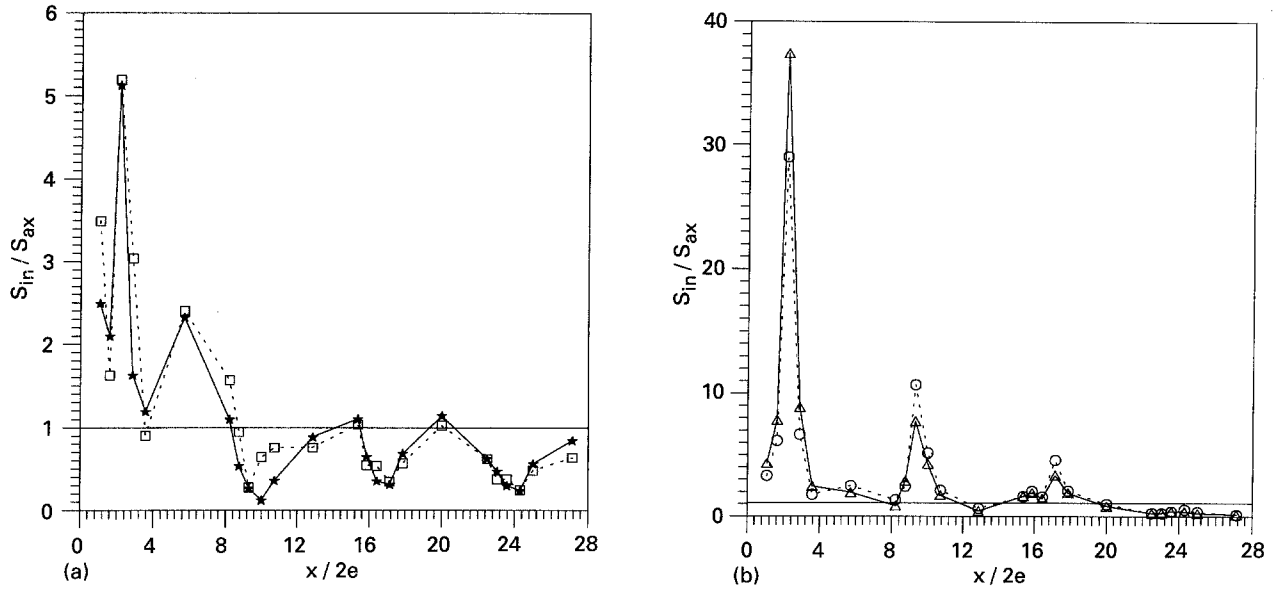


Fig. 6. Influence of the dimensionless axial location, $x/2e$, on velocity gradients on the inner cylinder in terms of $s_{in}/s_{ax}$: (a) laminar flow regime; (b) turbulent flow regime. Reynolds number, *Re*: (★) 295 and (□) 535 for (a); (△) 3300 and (○) 4060 for (b).

swirling flow on the inner core of the annulus, $s_{in}$, to that obtained in fully developed axial flow, $s_{ax}$ [11], is plotted as a function of the reduced location of the microcathodes, $x/2e$. One can see that the evolution of $s_{in}/s_{ax}$ along the flow path is more chaotic than that observed on the outer cylinder (Fig. 3). The velocity gradient does not decrease monotonically, but exhibits maxima and minima which are more pronounced in the laminar swirling flow regime (Fig. 6(a)). This evolution of $s_{in}/s_{ax}$ means that the resulting velocity, $T$, on the inner cylinder is not constant in magnitude and direction along the flow path. Some secondary vortices may appear on the inner cylinder which are not detected on the outer one using wall shear stress measurements. This flow structure is in keeping with the simulation [8]. In Fig. 6, there are many axial positions for which $s_{in}/s_{ax} < 1$, thus $T$ is lower in magnitude than the corresponding axial velocity in fully developed axial flow. The flow pattern on the inner cylinder will be more fully investigated using correlation and spectrum analysis to characterize the phenomena detected in the present study.

### 4.2. *Flow visualization results*

In Fig. 7, $\theta$, measured on the inner cylinder, as a function of $x/2e$, for $\psi = 0$ and different values of *Re* in the laminar swirling flow regime is plotted. The evolution of $\theta$ is seen to be very chaotic at the lower end of the cell: $\theta$ can be either positive or negative, which means that recirculation regions exist which persist higher up the cell when *Re* is increased. These observations are in keeping with wall shear stress data plotted in Fig. 6. Thus the flow pattern on the inner cylinder is very different from that on the outer one.

Figure 8 illustrates the influence of $\psi$, the angle with respect to the tangential inlet axis, on $\theta$ for $Re = 1500$.

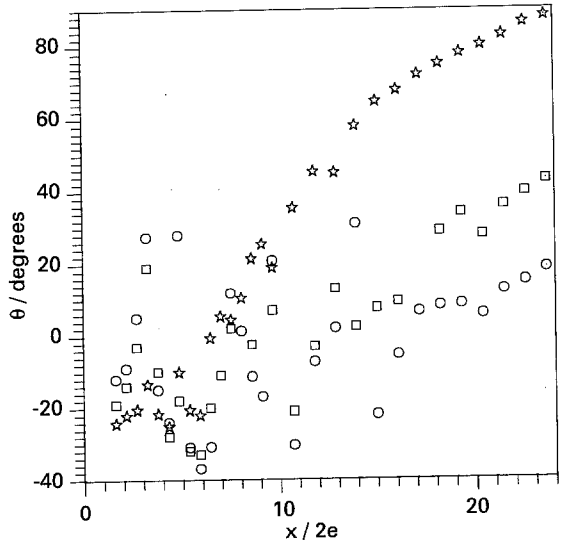


Fig. 7. Variation of the streamline angle, $\theta$, as a function of $x/2e$, for $\psi = 0$, on the inner cylinder. Reynolds number, *Re*: (☆) 233, (□) 988 and (○) 1994.

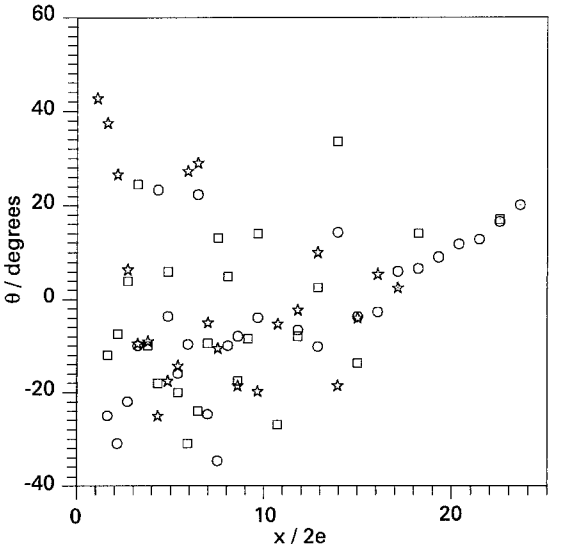


Fig. 8. Influence of the circumferential location, $\psi$, on the streamline angle, $\theta$, for $Re = 1990$ on the inner cylinder. $\psi$: (☆) $3\pi/2$, (□) $\pi$ and (○) $\pi/2$.

This graph clearly shows the three-dimensional structure of the flow field on the inner cylinder.

## 5. Conclusion

This first attempt to investigate the local flow field on both cylinders of an electrochemical cell fitted with a tangential inlet, equal in diameter to the gap thickness, has revealed some hydrodynamic characteristics of such a configuration:

(i) at the bottom of the cell, the flow field is strongly three-dimensional on both cylinders;
(ii) monotonic swirl flow is obtained farther from the entrance on the inner cylinder than on the outer one; and
(iii) the flow field on the inner cylinder appears to be very complex with recirculation zones.

This experimental study will be followed by a fuller investigation and analysis of flow characteristics in order to determine the location and the size of the recirculating flows using multisegmented electrochemical probes coupled with the dot-paint method.

## References


[1] A. K. Gupta, D. J. Liley and N. Syred, 'Swirl Flows', Abacus Press, Tunbridge Wells, UK (1984).
[2] D. Burfoot and P. Rice, *Chem. Engng. Res. Des.* **62** (1987) 128.
[3] R. Sethumadhavan and M. Raja Rao, *Int. J. Heat Mass Transfer* **26** (1983) 1833.
[4] R. F. Lopina and A. E. Bergles, *J. Heat Transfer* **91** (1969) 434.
[5] F. C. Walsh and G. Wilson, *Trans. IMF* **64** (1986) 55.
[6] P. Legentilhomme and J. Legrand, *J. Appl. Electrochem.* **20** (1990) 216.
[7] *Idem, Int. J. Heat Mass Transfer* **34** (1991) 1281.
[8] *Idem, Can. J. Chem. Engng.* **71** (1993), 299.
[9] J. Legrand, P. Legentilhomme, H. Aouabed, M. Ould-Rouis, C. Nouar and A. Salem, *J. Appl. Electrochem.* **21** (1991) 1063.
[10] L. P. Reiss and T. J. Hanratty, *AIChEJ.* **9** (1963) 154.
[11] T. K. Ross and A. A. Wragg, *Electrochim. Acta.* **10** (1965) 1093.
[12] N. Hay and P. D. West, *J. Heat Transfer* **97** (1975) 411.
[13] H. Yukawa and M. Hashimoto, *J. Chin. Ins. Chem. Eng.* **13** (1982) 161.
[14] R. J. Edwards, K. Jambunathan and B. L. Button, *Proc. Int. Heat Transfer Conf., Jerusalem* **5** (1990) 401.
[15] M. Benisec, *Zammz. Agew. MU Mech.* **61** (1981) 138.
[16] M. Benisec, Z. Protic and M. Nedeljkovic, *Zammz. Agew. MU Mech.* **66** (1984) 195.
[17] O. Kato and T. Kato, *Bull. Jap. Soc. Mech. Engrs.* **230** (1984) 1659.